

Forming disc galaxies in major mergers: III. The effect of angular momentum on the radial density profiles of disc galaxies

N. Peschken^{1,2*}, E. Athanassoula¹, S. A. Rodionov¹

¹Laboratoire d'Astrophysique de Marseille, 38, rue Frédéric Joliot-Curie 13388 Marseille cedex 13 FRANCE

²Nicolaus Copernicus Astronomical Center, Polish Academy of Sciences, ul. Bartycka 18, 00-716 Warsaw, Poland

6 March 2017

ABSTRACT

We study the effect of angular momentum on the surface density profiles of disc galaxies, using high resolution simulations of major mergers whose remnants have downbending radial density profiles (type II). As described in the previous papers of this series, in this scenario, most of the disc mass is acquired after the collision via accretion from a hot gaseous halo. We find that the inner and outer disc scalelengths, as well as the break radius, correlate with the total angular momentum of the initial merging system, and are larger for high angular momentum systems. We follow the angular momentum redistribution in our simulated galaxies, and find that, like the mass, the disc angular momentum is acquired via accretion, i.e. to the detriment of the gaseous halo. Furthermore, high angular momentum systems give more angular momentum to their discs, which affects directly their radial density profile. Adding simulations of isolated galaxies to our sample, we find that the correlations are valid also for disc galaxies evolved in isolation. We show that the outer part of the disc at the end of the simulation is populated mainly by inside-out stellar migration, and that in galaxies with higher angular momentum, stars travel radially further out. This, however, does not mean that outer disc stars (in type II discs) were mostly born in the inner disc. Indeed, generally the break radius increases over time, and not taking this into account leads to overestimating the number of stars born in the inner disc.

Key words: galaxies: spiral – galaxies: structure – galaxies: kinematics and dynamics

1 INTRODUCTION

The early pioneering work of Freeman (1970) showed clearly that the radial surface density profile of disc galaxies is well fitted by an exponential. Later work (Van der Kruit 1979, and later e.g. Pohlen et al. 2002; Erwin, Beckman & Pohlen 2005; Gutiérrez et al. 2011) revealed the presence of a break in the profile of most galactic discs, as well as the fact that both the inner and the outer parts are well described by exponentials.

The break can be of two kinds, depending on the scalelengths of the two exponentials. If the slope of the outer part of the disc, hereafter called outer disc, is steeper than the slope of the inner part (inner disc), i.e. if the inner disc scalelength is greater than the outer disc one, the profile is called downbending, or type II (Pohlen & Trujillo 2006). This is the most common profile for disc galaxies (e.g. Pohlen & Trujillo 2006; Azzollini, Trujillo & Beckman 2008; Laine et al.

2014). In the opposite case, the outer disc is shallower than the inner disc, and the profile is called upbending, or type III. The single exponential case, where no break is observed, is called type I.

Several mechanisms producing those different types of discs have been proposed so far. While it has been argued that a single exponential is the canonical profile for a disc (Gunn 1982; Lin & Pringle 1987; Yoshii & Sommer-Larsen 1989; Ferguson & Clarke 2001; Elmegreen & Struck 2013, 2016; Herpich, Tremaine & Rix 2016; Struck & Elmegreen 2017), many formation scenarii have been proposed for the downbending discs, sometimes related to each other. They are thought to be created by bars via the Outer Lindblad Resonance (Debattista et al. 2006; Pohlen & Trujillo 2006; Muñoz-Mateos et al. 2013; Kim et al. 2014), by star formation thresholds (Schaye 2004; Pohlen & Trujillo 2006; Elmegreen & Hunter 2006), or connected with morphological components such as rings or spirals (Laine et al. 2014). Stellar migration is also found to be important in the creation of type II profiles, being able to

* Contact e-mail: npeschken@camk.edu.pl

redistribute stars from the inner disc to the outer disc, and can be coupled with a star formation threshold (Roškar et al. 2008). On the other hand, type III profiles (upbending discs) remain poorly understood. They are sometimes associated with a spheroidal component such as a stellar halo, or with the superposition of a thin and a thick disc, and could be the result of minor mergers, or be linked to a strong bar (Erwin et al. 2005; Younger et al. 2007; Bakos & Trujillo 2012; Comerón et al. 2012; Herpich et al. 2015b).

Although the majority of the present-day spirals is thought to have experienced at least one major merger in their history (e.g. Hammer et al. 2009), so far most of the simulated galaxies used to investigate the formation of these different disc types have been evolved in isolation. Recently, however, we presented in Athanassoula et al. (2016, hereafter A16) three fiducial examples from a large sample of high resolution simulations of a major merger between two disc galaxies with a hot gaseous halo each, and showed that the remnants are good models of spirals. In this paper, we aim to study the role of angular momentum in shaping type II profiles, obtained from our large sample of major merger simulations.

The outline is as follows. In section 2, we briefly summarise the necessary parts of A16, and describe the fitting procedure for the radial density profiles. We compute the initial angular momentum and link it to the scalelengths in section 3. In section 4, we follow the angular momentum redistribution to explain how the initial angular momentum can affect the final disc properties. We discuss our results in section 5, and conclude in section 6.

2 TECHNICAL ASPECTS

2.1 Description of the simulations

In this section, we will briefly summarise the simulations characteristics, which have been obtained and described in some detail in A16. Our simulations start from two spherical protogalaxies consisting only of dark matter (DM) and hot gas, which we set on a given orbit. We use a total of 5.5 million particles (2 million for the baryons, 3.5 million for the DM), with softenings of 25 pc for the gas and 50 pc for the DM. Each particle’s mass is $5 \times 10^4 M_\odot$ for the gas and stars, and $2 \times 10^5 M_\odot$ for the dark matter. By the time of the merging, a disc has formed in each of the progenitors, which is destroyed by the merging, its stars ending up mainly in a classical bulge. Gas continues to fall from the halo, and new discs, both thin and thick, are gradually formed in the remnant. Well-defined spiral arms soon develop in the thin disc, as well as a bar and a boxy/peanut bulge. Each simulation ends after 10 Gyr evolution, showing a remnant with a classical bulge-to-total ratio which is consistent with that of real spiral galaxies.

Our simulations are made using the N-body/SPH code GADGET3, including gas and its physics. The description of this code can be found in Springel & Hernquist (2002) and Springel (2005). Stars and dark matter are modeled by N-body particles, and gas by SPH particles, with fully adaptive smoothing lengths. Gravity is computed with a hierarchy tree algorithm, and the code uses subgrid physics for the feedback, star formation and cooling, described in Springel & Hernquist (2003).

For a description of the technical aspects of the simulations we refer the reader to Rodionov, Athanassoula & Peschken (2017, hereafter R17). To avoid an excessive central concentration in our simulated galaxies, which would lead to unrealistic circular velocity curves and would delay the formation of the bar, we added AGN feedback (R17). This is based on a density threshold ρ_{AGN} and a temperature T_{AGN} , while the physics underlying it is described in detail in A16.

The simulations have a variety of different orbits for the two merging protogalaxies. These orbits are characterised by their ellipticity, and the initial distance between the two progenitors. Each orbit leads to a different merging time, which is difficult to define precisely, but can be approximated by deriving the time beyond which the distance between the two centers of density stays below 1 kpc (see A16).

The two protogalactic haloes start with an initial spin, characterised by a spin value f representing the fraction of particles rotating with a positive sense of rotation. Thus for $f = 1$, all the particles rotate in the direct sense, while for $f = 0.5$ there is no net rotation.

The simulations used in this paper have rather early merging times, i.e. between 1.2 and 2.2 Gyr after the start of the simulation. About two thirds of our simulations have spin axes perpendicular to the orbital plane, but for the other simulations we tilt one or both protogalaxies by a chosen angle, to see the effect of the spin axis orientation. In most simulations the spin value f is the same for both protogalaxies, but in some simulations we introduced a different spin in each protogalaxy. We ran simulations of mergers with mass ratios between the two protogalaxies of 1, 1/2, 1/3, 1/4 and 1/8.

A central AGN is present in the remnant galaxy of the majority of our simulations, as described in A16 and R17, but we include 21 simulations without AGN to cover a larger part of the available parameter space. Nevertheless, the presence of our AGN affects mainly the central part of the disc (R17), and thus should not have an impact on the analysis presented in this paper.

We will first consider a subsample of 132 simulations which all have the same total mass, i.e. the same number of particles (5.5 million), and call it sample A. We also ran 67 simulations with various masses, each different from the mass of the simulations in sample A. This is done by keeping the same mass for single particles, but changing the number of particles. We add this group of 67 simulations (called sample B) to sample A to obtain a new sample of 199 simulations, sample A+B, which we will use in the discussion (section 5.2).

2.2 Fitting the radial density profiles

To derive the stellar radial density profile, we use axisymmetric concentric cylindrical annuli, and choose $z_{lim}=1$ kpc as maximum height to keep only the thin disc profile. As shown in A16, the disc at the end of our three fiducial simulations is composed of an inner and a downbending outer disc (type II), separated by a break. This is also the case for the 199 simulations of the sample used in this paper (sample A+B), therefore we fit the disc part of our profiles with two exponential functions. We use a “piecewise” fit, which means

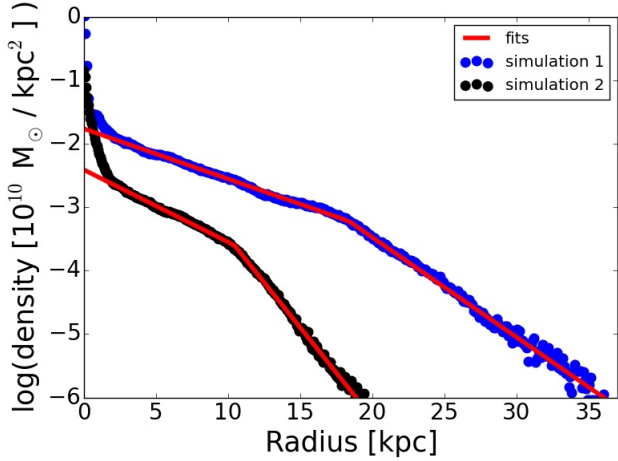


Figure 1. Projected surface stellar density radial profiles for two simulations, together with the corresponding fits for the disc part. For clarity, the second simulation (in black) has been shifted down by 1 logarithmic unit. Simulation 1 has a higher initial spin parameter λ than simulation 2.

that we fit the inner and the outer disc separately with an exponential:

$$\Sigma_{in}(R) = \Sigma_i \exp\left(\frac{-R}{h_i}\right), \quad R < R_{break} \quad (1)$$

$$\Sigma_{out}(R) = \Sigma_o \exp\left(\frac{-R}{h_o}\right), \quad R > R_{break} \quad (2)$$

where Σ_i , Σ_o are normalization factors, h_i and h_o are the inner and outer disc scalelengths, and R_{break} the break radius. The latter is derived by taking the intersection between the inner and the outer disc fits. The interval to fit for each part of the disc is selected manually, and we exclude, after visual inspection, every simulation for which the fit is not reliable. Two examples of fits are shown in Fig. 1. Another way to make this fit would be to use a double exponential function (or “broken-exponential”) for the whole disc, which has been shown to give very similar results (differences in the scalelengths < 5 per cent, Erwin et al. 2008). We chose the present approach because of its simplicity.

The scalelengths and the break radius change with time, as shown both by observations (Perez 2004; Azzolini et al. 2008), and simulations (Roškar et al. 2008; Athanasoulas, Peschken & Rodionov, in prep, hereafter Paper IV), and to be able to compare consistently the scalelengths derived for the different simulations, we need to compare all galaxies at the same evolutionary time, i.e. at the same time after the merging. We thus take a fixed evolution time of 7.8 Gyr after the merging for every simulation. Given that the merging times have values between 1.2 and 2.2 Gyr, the times at which we now study the disc are therefore between 9 and 10 Gyr, depending on the simulation. We will hereafter refer to this time as the final state.

We here aim to investigate the role of angular momentum in the formation of the new disc formed after the merging, in the secular evolution period of the galaxy. Nevertheless, some of the stars formed before or during the merging were

spread all over the galaxy by the merging, and can pollute our density profiles. These stars represent between 10 and 30 per cent of the total stellar mass in the thin disc. Most of them are located in the bulge region (about 65 per cent), but they can also form a stellar halo or a thick disc, which will add particles to the thin disc, changing the value of the scalelengths by up to 20 per cent. These stars are not related to the disc formation and its dependence on the angular momentum, and we thus chose to remove them, selecting only the stars formed after the merging to derive our density profiles and the corresponding scalelengths.

3 THE ROLE OF ANGULAR MOMENTUM

3.1 Definition of the global, dimensionless spin parameter

Here, we use the dimensionless spin parameter λ (Peebles 1969):

$$\lambda = \frac{L|E|^{1/2}}{GM^{5/2}}, \quad (3)$$

where L , E and M are respectively the total angular momentum, energy and mass of the system including its dark matter, gas and stars, computed with respect to the center of mass of the system, and G is the gravitational constant. The total energy is computed adding the kinetic energy, the gravitational potential energy and the gas internal energy. The total angular momentum L is a conserved quantity, but the total energy varies with time because of processes such as the cooling of the gas and the stellar feedback. We therefore have to specify the time at which we will calculate λ , and make sure it is calculated consistently for all simulations. To avoid the technical difficulties inherent in using the merging time, we use $t=1$ Gyr before the merging, which we call the initial state.

3.2 Angular momentum and scalelengths

How does the disc structure relate to the global spin parameter λ ? From the definition of angular momentum, we expect that for two galaxies of the same total mass, the galaxy with the highest angular momentum will be more extended, as it has been shown in previous studies (e.g. Dalcanton, Spergel & Summers 1997 and Kim & Lee 2013). We checked this result in our simulations by plotting the size of our galactic discs at the final state as a function of λ , for the simulations of sample A. As an estimate of the disc size, we take R_{95} , the cylindrical radius containing 95 per cent of the total stellar mass. We can see on Fig. 2 that the size of the final galaxy increases linearly with λ , with a high correlation coefficient.

We thus find the disc to be globally larger for high λ galaxies, as expected. However, since the disc is constituted of an inner and an outer part, which part of the disc is affected most? We expect at least one of the two discs (inner or outer) to be larger at higher λ . To have a first insight of the effect of the spin parameter λ on the parameters of the radial density profiles, we plot in Fig. 1 the profiles at the final state (as defined in section 2.2) for two simulations of sample A with different λ values. We can see that the scalelengths of the simulation with a higher λ (in blue) are

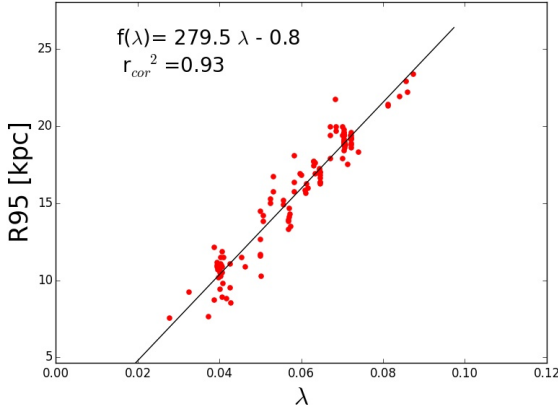


Figure 2. Cylindrical radius containing 95 per cent of the stellar mass at the final state, as a function of the spin parameter λ computed at the initial state, for the simulations of sample A. The corresponding linear fit is plotted in black, with the equation and correlation coefficient given in the top left corner.

larger, and its break is located further out. The next step is to see whether this preliminary result is valid for all the simulations in sample A, as described below.

We examine the discs of the remnants at the final state, and plot the three parameters derived from the fits of the radial density profiles (inner, outer disc scalelength and break radius) as a function of the initial λ for each simulation in sample A (Fig. 3). As described in section 2.2, we excluded all the simulations for which there was some uncertainty in the fit of the corresponding parameter, which explains why the number of points is different for each plot. We thus have a total of 97 values for the inner disc scalelength (hereafter inner scalelength), 99 for the outer disc scalelength (outer scalelength) and 84 for the break radius (for which the fits of both the inner and the outer disc have to be reliable).

We see that the inner scalelength, the outer scalelength and the break radius *all* increase linearly with λ , so that larger angular momentum systems produce discs with larger inner, outer scalelengths and break radii. This confirms the results of [Herpich et al. \(2015a\)](#) for the inner scalelength and the break radius for cases with isolated galaxies with no mergers (see discussion in section 5.1), and adds a further argument showing that the remnant of a major merger possesses all the characteristics of a disc galaxy.

The correlations of the fits in Fig. 3 are tight, especially for the break radius. The scalelengths show a larger spread, presumably because their values can be more strongly influenced by the presence of morphological components such as bars, spirals or rings than the break radius.

It is important to note that all the simulations we have so far considered (sample A) have identical total masses (gas + stars + DM) and similar total stellar masses at their final state, so that the spread of scalelengths cannot be simply due to a mass dependence. Thus the spread should be due to the different parameters of the initial conditions in the various simulations, such as the halo spin value, and, in particular, to the different orbits of the two progenitors.

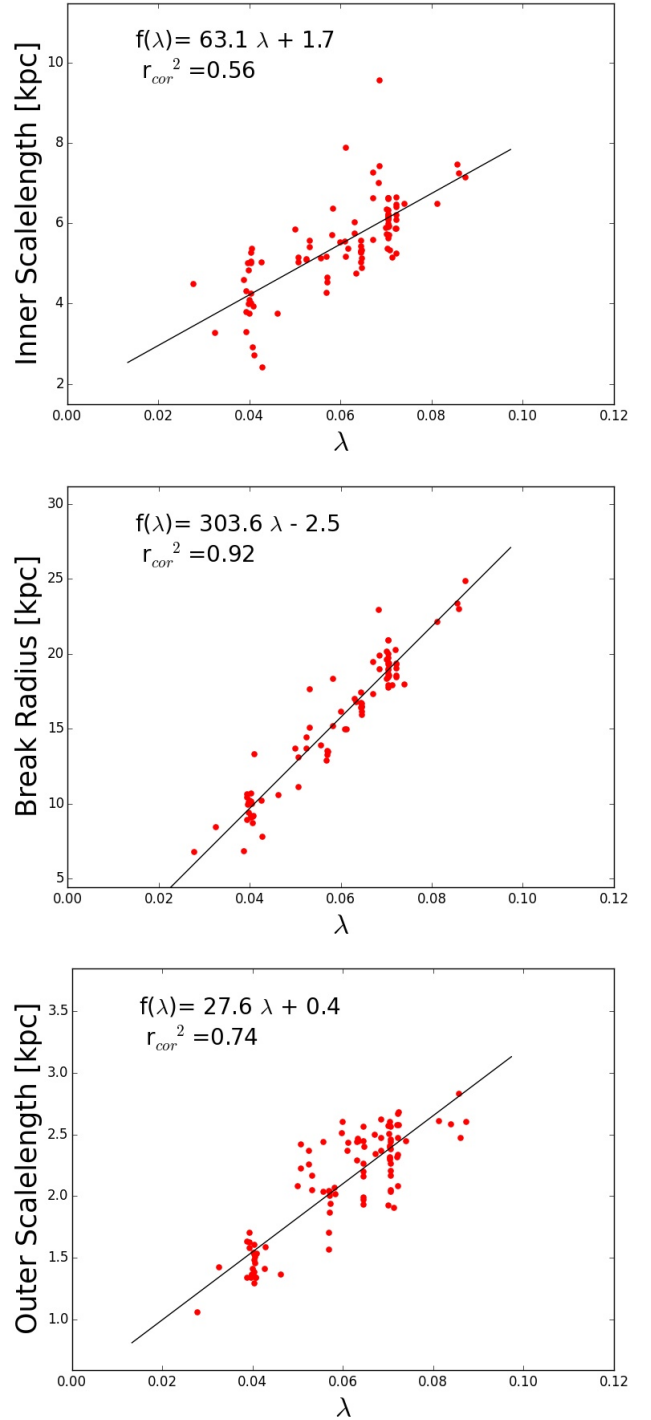


Figure 3. From top to bottom we plot respectively the inner scalelengths, the break radii and the outer scalelengths derived from the fits at the final state, each as a function of the spin parameter λ taken at the initial state, for the simulations in sample A. The corresponding linear fits are plotted in black, with the equation and correlation coefficient given in the top left corner of each plot.

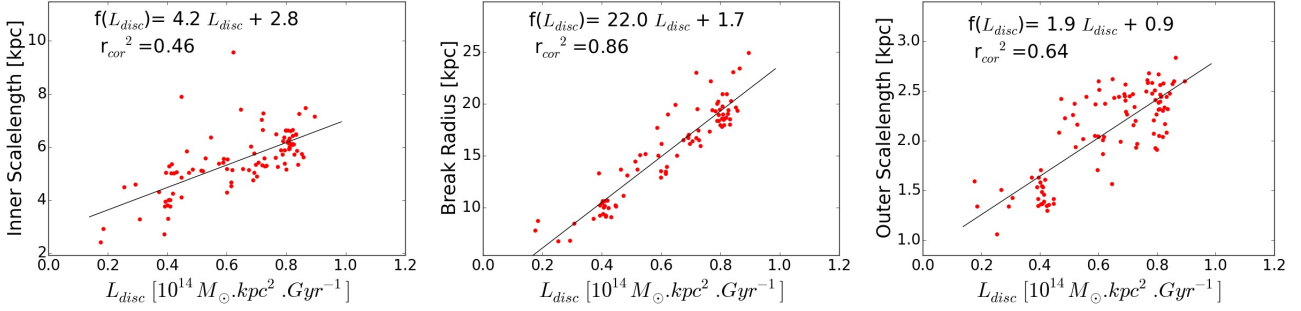


Figure 4. Correlations of the inner scalelength, the break radius and the outer scalelength, with the total baryonic angular momentum of the final disc, for sample A.

4 UNDERSTANDING OUR CORRELATIONS

The dimensionless spin parameter λ is computed 1 Gyr before the merging, and is dominated by the halo (hot gas and DM), because the discs of the protogalaxies are of short extent and of low mass, as the merging occurs early in our sample of simulations. Therefore, λ does not seem to be directly related to the final disc of the remnant and to its properties such as the scalelengths. To understand how it can yet influence the final disc, we will first look at the angular momentum in the final disc.

4.1 Angular momentum in the baryonic disc

We define the baryonic disc as the 2 kpc thick pill-box ($|z| < 1$ kpc, consistently with section 2.2) of maximum radius $R_{max} = 1.5 R_{break}$, and exclude the inner 3 kpc to remove the bulge part. We then compute the total angular momentum of the baryonic matter (gaseous + stellar particles) in this volume at the final state, and plot it against the scalelengths and the break radius for all the simulations of sample A in Fig. 4. We find clear correlations, showing that the properties of the disc are directly linked to its angular momentum.

We now need to relate this disc angular momentum to the initial halo-dominated spin parameter λ . We showed in A16 that the gas from the gaseous halo accretes onto the disc and thus rebuilds it after the merger, by fuelling star formation in the disc throughout the whole simulation. We suggest here that gas accretion from the halo is the main mechanism gradually transferring angular momentum from the gaseous halo to the disc, and investigate this in the following subsections.

4.2 Angular momentum redistribution

To be able to study the exchanges of angular momentum between the disc and the gaseous halo, we first made sure that the angular momentum exchanges between the baryonic and the dark matter haloes are relatively small and thus can be neglected in the context of our very simple qualitative explanation. Indeed, we found such exchanges to be of the order of few per cent.

To illustrate the angular momentum exchanges in our simulations, we will focus on two fiducial simulations of sample A, *mdf732* and *mdf780*, presented in A16, which have quite

different λ values, *mdf732* having a considerably higher λ than *mdf780*. Note, however, that we made the same analysis with other simulations as well, and found similar results.

We define the disc as in section 4.1, and the halo as everything else. The baryonic halo is mainly constituted of gas, but a few stars are expected to be found as well. Nevertheless, we find the total angular momentum L of these stars to be a thousand times lower than the halo gas, and we thus neglect them.

We first plot in Fig. 5 the evolution over time of the total mass of the halo gas, the disc gas and the stars in the disc, separately. As expected (A16), the gaseous halo loses mass while the stellar disc gains it. In Fig. 6 we further plot the angular momentum as a function of time for these three components, and we can see that the halo gas is gradually losing angular momentum over time, while the angular momentum of the stellar disc is increasing. The gas in the disc is losing mass and angular momentum due to star formation in the disc. These plots thus show how the gas in the halo is accreted onto the disc, where it forms stars (see A16). Therefore, the stellar disc is gaining angular momentum by gas accretion and star formation.

Note that this simple angular momentum redistribution picture implicitly assumes that our system is relatively isolated. Otherwise, it will be able to exchange matter and/or angular momentum with other galaxies, so that the total mass and angular momentum of our system need not be conserved quantities.

Thus, the disc grows from material taken from the gaseous halo, which directly gives a fraction of its angular momentum to the disc. To find how this fraction varies for different simulations, we plot (Fig. 7) the final baryonic disc angular momentum (as defined in section 4.1) versus the initial total baryonic angular momentum of the system (which in practice we calculate at the merging time). We find a clear correlation, which shows that gaseous haloes with more angular momentum create on average discs with more angular momentum.

To conclude, the initial properties of the halo – and in particular its angular momentum – affect the final disc structure via gas accretion, which constitutes a plausible reason for the disc properties (scalelengths and break radius) to be linked to the initial spin parameter λ .

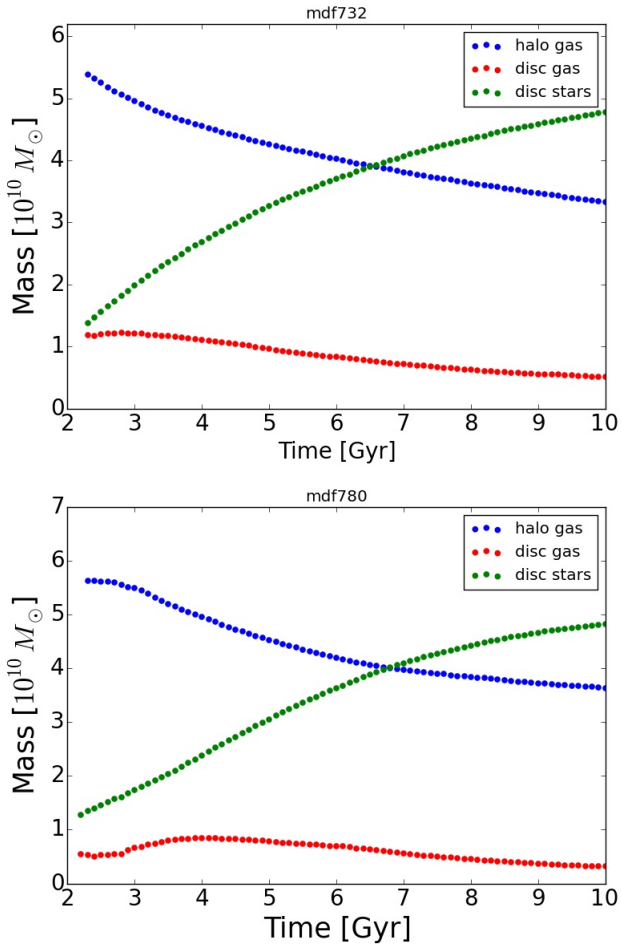


Figure 5. Total mass of the gaseous halo, the gaseous disc and the stellar disc as a function of time for two simulations, mdf732 (high λ , upper panel) and mdf780 (low λ , lower panel).

5 DISCUSSION

5.1 Robustness of the correlations

To test the robustness of our results with respect to the time defined as final state, we fitted the radial density profiles also 5.8 Gyr after the merging, instead of 7.8 Gyr. The values of the correlation coefficients are reported in Table 1 (2nd row). As expected due to the growth of the disc, the individual values of the scalelengths and the break radii are different, but we still find increasing linear trends with λ . Therefore, the time chosen as final state does not seem to be important for this study, provided it is consistent for all simulations and provided it is sufficiently long after the merging for the disc to have settled. Under these conditions, the increasing trend with λ should be valid regardless of the disc evolution time. We can thus keep 7.8 Gyr after the merging as the final state without being concerned about the effect of our choice.

We also changed the time at which we calculate λ (the initial state) and used the merging time. We found very little difference in the results, and the correlation coefficients are similar (Table 1, 3rd row). We repeated this analysis, calculating λ at various times covering the range between the

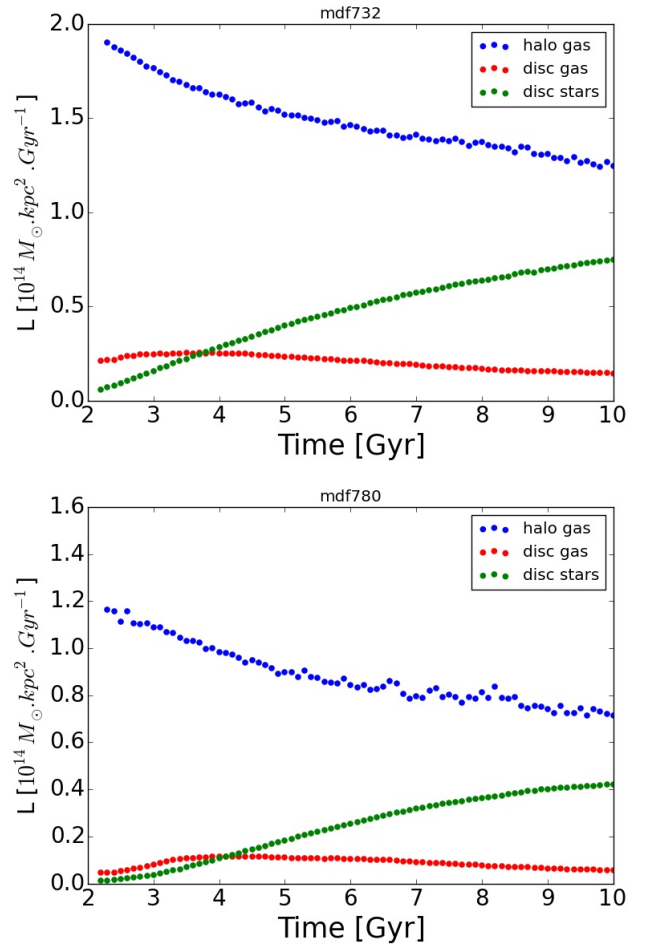


Figure 6. Total angular momentum of the gaseous halo, the gaseous disc and the stellar disc as a function of time for two simulations, mdf732 (high λ , upper panel) and mdf780 (low λ , lower panel).

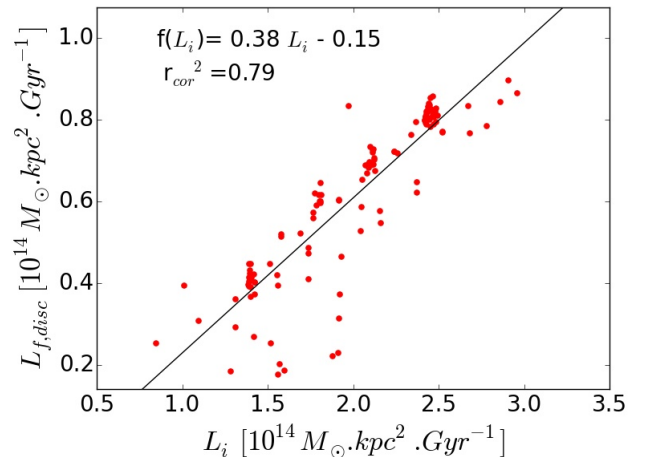


Figure 7. Final baryonic disc angular momentum, as a function of the total baryonic angular momentum of the system computed at the merging time, for simulations in sample A.

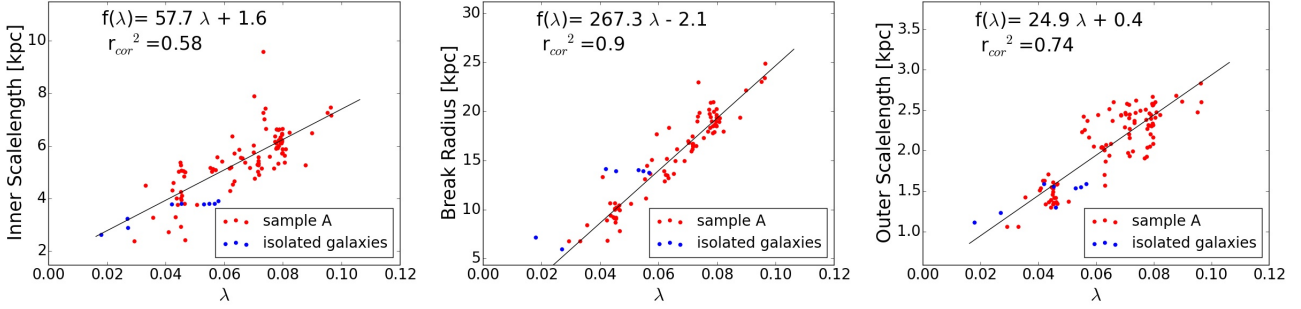


Figure 8. Same plots as in Fig. 3, but adding simulations of isolated galaxies (in blue).

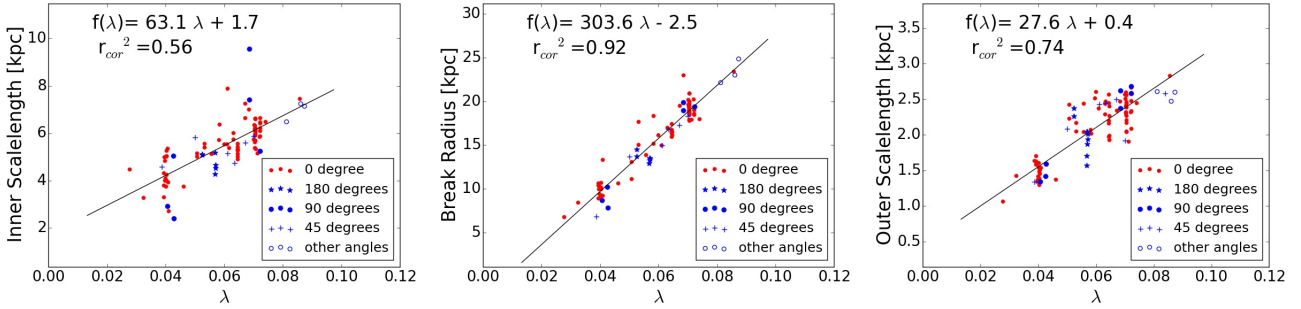


Figure 9. Same plots as in Fig. 3, but showing the effect of spin orientation on our correlations, with the angle between the two protogalaxies axes.

start of the simulation and the merging, and conclude that the time chosen does not change the results significantly. We can also use λ at the final state instead of the initial state, to link λ and the disc structure both taken at the same time. We found again the same increasing trends, with the correlation coefficients reported in Table 1 (4th row). This points out the existence of a correlation between the initial and final λ , which we confirmed by plotting one against the other, and argues that for an analysis of this type, one can take the value of angular momentum at any time, as long as it is consistent for all simulations.

We also used λ at $t=0$ Gyr for all simulations (sample A), and again find correlations for the scalelengths and the break radius, although the correlation coefficients are slightly lower (Table 1, last row).

To see if the results obtained for our merger simulations are also valid for isolated galaxies, we included 12 simulations which take only one of the protogalaxies used in the merger simulations, and see how it evolves in isolation. This protogalaxy contains the same number of particles as the simulations of sample A, to keep the same total mass. To be able to compare the merger to the isolated simulations, we define the initial state as the start of the new disc formation for both, i.e. at the end of the merging for the former, and at $t=0$ for the latter. We take 7 Gyr after the initial state as the final state. We find that the isolated galaxies fit well with the merger simulations (see Fig. 8), which argues that the increasing linear trends of the two scalelengths and the break radius with the angular momentum seem to be the same if the disc is formed in isolation or from a major merger. Our results should therefore also be valid for

isolated galaxies.

Herpich et al. (2015a) did a similar analysis to ours, looking at the dependence of the scalelengths and the break radii with the angular momentum, but using a sample of 9 simulations of galaxies evolved in isolation. They computed the spin parameter λ of the halo at the start of the simulation, and also found that the inner scalelength and the break radius increase with λ . However, they observed a decreasing trend of the outer scalelength with λ , while we have an increasing one. We explain this difference by the fact that they included upbending discs in their analysis, whose outer scalelengths are naturally much higher than for downbending discs, while we only have downbending discs in our sample. Upbending profiles will be discussed in detail in a future paper (Paper IV). As a consequence, Herpich et al. (2015a) find an increasing trend with λ for the ratio of the inner scalelength to the outer scalelength, while we do not, our values showing no correlation with λ .

We mentioned in section 2.1 that in some simulations, the spin axis of one or both protogalaxies is tilted by a given angle; this concerns 34 simulations in sample A. This angle can be around the X or the Y axis, Z being the axis perpendicular to the orbital plane. We wanted to see if these simulations behave differently in our results than the simulations where both protogalactic spin axes are parallel, and perpendicular to the orbital plane. In Fig. 9 we plotted again our correlations between the scalelengths and λ , but showing the effect of spin orientation. We can see that the simulations where the spin axes are not parallel (angle $\neq 0$) fit reasonably well

Table 1. Parameters of the linear fits for different plots of λ versus the inner scalelength, break radius and outer scalelength. t_i , t_f and t_{merg} are respectively the times of the initial state, the final state and the merging, and r_c^2 is the correlation coefficient for the linear fit with equation: $f(\lambda) = a\lambda + b$.

	Inner Scalelength			Break Radius			Outer Scalelength		
	r_c^2	a	b	r_c^2	a	b	r_c^2	a	b
$\lambda_{t=t_i}, t_f = t_{merg} + 7.8$	0.56	63.1	1.7	0.92	303.6	-2.5	0.74	27.6	0.4
$\lambda_{t=t_i}, t_f = t_{merg} + 5.8$	0.48	55.0	2.3	0.91	283.5	-1.9	0.74	24.8	0.4
$\lambda_{t=t_{merg}}, t_f = t_{merg} + 7.8$	0.56	58.0	1.7	0.90	277.9	-2.2	0.72	24.9	0.5
$\lambda_{t=t_f}, t_f = t_{merg} + 7.8$	0.55	54.0	1.6	0.90	259.8	-3.0	0.73	23.7	0.4
$\lambda_{t=t_f}, t_f = t_{merg} + 5.8$	0.47	47.0	2.2	0.87	238.6	-1.8	0.71	20.9	0.4
$\lambda_{t=0}, t_f = t_{merg} + 7.8$	0.53	59.8	2.0	0.89	291.1	-1.1	0.72	26.6	0.6

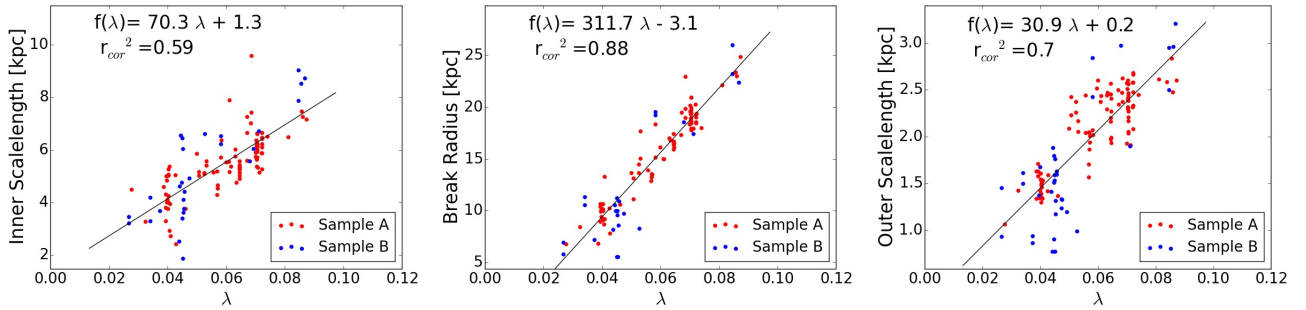


Figure 10. Same plots as in Fig. 3, but adding a sample of 67 simulations (sample B) with total masses different from those of the simulations in sample A.

with the others. We can thus conclude that our results seem to be valid regardless of the spin axis orientation.

We also looked at the effect of the presence of a central AGN on our correlations, and found that the simulations without AGN also fit well with the ones having an AGN. This confirms that our AGN only affects the central part of the galaxy (R17).

The effect of the initial density distribution of gas and DM have also been tested since our sample contains simulations with different distribution parameters, such as the initial characteristic radii of the halo (see A16) or the presence of a central core for DM. Although the corresponding parameter space is very large, our relatively few trials argue that such parameters do not seem to have an effect on the correlations we found. Various other parameters, such as the merging orbit, the baryonic to total mass ratio, and the softening of the gas and DM, were also shown to have no significant impact on our results.

5.2 Introducing simulations with different total masses

Here we will analyse the effect of changing the total mass in the simulations, using sample B (see section 2.1). The problem when analysing simulations of different masses is that the evolution time-scale is also different. In our analysis we took a fixed evolution time after the merging (7.8 Gyr) to compare the properties of the disc, which introduces a small

inconsistency when we compare simulations with different total masses.

Nevertheless, we expect the time-scales to be similar if the total masses are not too different, which is the case of the simulations in our subsample of 67 galaxies (sample B) since they have total masses between 0.5 and 2 times the total mass of simulations in sample A. We include them in our correlations (Fig. 10) and find again high correlation coefficients; the sample B fits well with sample A. Furthermore, we added simulations of galaxies evolved in isolation as in section 5.1, but with half the number of particles, i.e. with a mass twice lower than the simulations of sample A. We found that these simulations match well in the correlations, which again suggests that our results are valid also for galaxies formed in isolation. Moreover, we included the simulations of sample B in the correlation of the final baryonic disc angular momentum as a function of the initial baryonic angular momentum (as in Fig. 7), and found again a very good match.

Since the simulations of sample B follow similar trends as sample A despite their total masses being different, in the following subsections we will include them in our analysis, using the A+B sample.

5.3 Migration and angular momentum

The formation of outer discs in downbending profile galaxies is still debated, but one of the main possible scenario relies on the presence of outwards stellar migration to build the

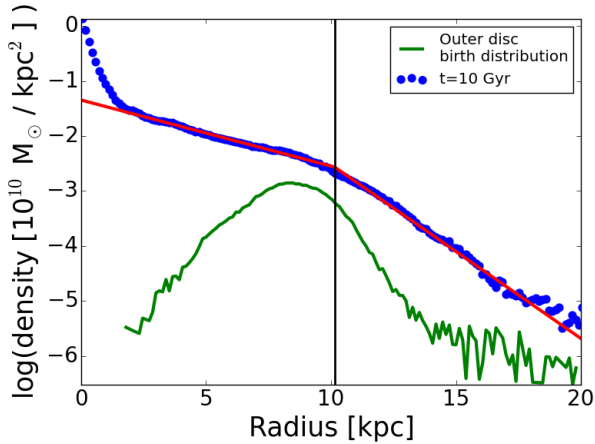


Figure 11. Radial density profile for a snapshot at $t=10$ Gyr (in blue), and distribution at time of birth of the stars ending up in the outer disc (in green). The fit of the profile at $t=10$ Gyr is plotted in red, and the corresponding break radius is indicated with a black vertical line.

outer disc (Roškar et al. 2008). We thus investigate where the stars in the outer disc of our remnant galaxies come from, by calculating the radius at which they were born. The stellar discs of the two protogalaxies are separate before the collision and thus the birth radius with respect to the remnant galaxy cannot be defined. We therefore use in our analysis only the stars born after the merging, as in section 2.2.

We define at any given time the stars of the outer disc as all the stellar particles located beyond the break. We plot in Fig. 11 the distribution of the radii at birth of the stars which by $t=10$ Gyr end up in the outer disc, for simulation *mdf730* from sample A, which was chosen because of its smooth profile, allowing us to make our points on migration clearer. Since every star is born at a different time, this distribution does not represent a real stellar distribution at any time of the simulation, but it helps visualise the fraction of stars born at a given radius throughout the whole simulation. We can see that most stars of the outer disc (78 ± 18 per cent for sample A+B) were born at a radius less than the break radius found at $t=10$ Gyr. This means that these stars have migrated radially outwards to form the outer disc, establishing the presence of inside-out stellar migration in the disc. This is in agreement with the results of Roškar et al. (2008) presenting simulations with a downbending disc profile induced by a star formation threshold and outward migration, and with observations e.g. in Radburn-Smith et al. (2012) and Zheng et al. (2015), and thus adds a further argument to those presented in A16 that the remnant of a major merger is a disc galaxy and behaves in all aspects as such.

Having established that there is inside-out stellar migration in our discs, we explore the effect of angular momentum on this phenomenon. To characterise the migration, we calculate the distances travelled by these stars migrating towards the outer disc, throughout the whole simulation. To derive the migration distances for a given simulation, we first compute the radial distance travelled by each star ending up

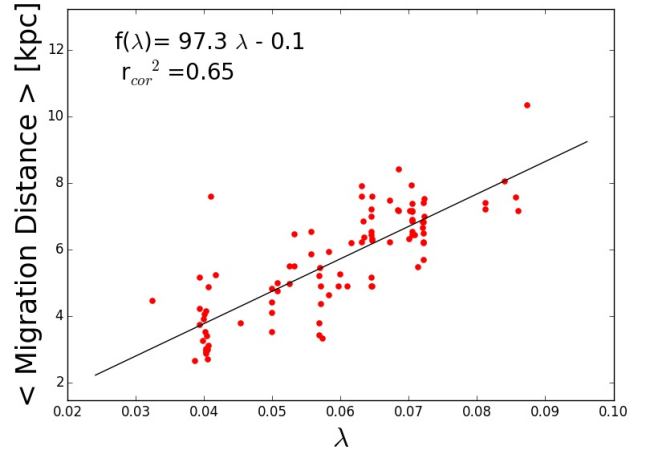


Figure 12. Mean inside-out migration distance of the stars ending up in the outer disc, as a function of the initial spin parameter λ , for sample A+B.

in the outer disc between its time of birth and the final state (as defined in section 2.2):

$$D_{mig} = R_{final} - R_{birth}, \quad (4)$$

where R_{final} and R_{birth} are the radii at the final state and at birth for each star. We remove again the stars born before the merging since migration only starts after the collision, or, more precisely, after the disc formation begins (t_{bd} , A16). Since we are only interested in the outward migration towards the outer disc, we also remove the stars migrating inwards, which represent only about 5 per cent of the outer disc population. We then take the mean over all the remaining stars to get a single value for each simulation, which we plot versus λ . We repeat this for all the simulations in sample A+B and plot the result in Fig. 12. We see a clear increasing trend of the migration distances with λ , allowing us to conclude that higher initial angular momentum systems lead to discs with higher migration distances towards the outer disc. In fact, we find the same result if we consider inside-out migration in the whole disc, and do not restrict ourselves to outer disc stars. The stars travel globally further out in high angular momentum systems, and this is particularly important in the outer disc, where $94 (\pm 5)$ per cent of the stars have undergone inside-out migration (compared to 46 ± 5 per cent for the whole disc).

The angular momentum thus seems to play an important role in the radial outward migration, by redistributing the stellar content in the outer disc efficiently (with large travelling distances) or not.

This result is consistent with outer discs in high λ simulations having larger scalelengths: if stars travel further out, their final distribution will be more extended, resulting in a larger outer disc.

5.4 Migration and birth radius

In section 5.3, we showed that most particles ending up in the outer disc were born inside the break radius, as calcu-

lated at $t=10$ Gyr. However, the stars whose birth distribution has been plotted in Fig. 11 were born at all times after the merging. As will be shown for our simulations in Paper IV (see also Perez 2004 and Azzollini et al. 2008 for observations), the break radius generally increases with time, so that stars which are born inside the 10 Gyr break in Fig. 11 could in fact be born beyond the break taken at their time of birth. Therefore, we cannot claim that about 80 per cent of the outer disc's stars that were born at a radius which corresponds to the inner disc at 10 Gyr were actually born in the inner disc, since their birth radius could be in the outer disc at their birth time. Although this does not change the fact that most of these stars clearly migrated outwards, it could question the claim that they travelled from the inner disc to the outer disc.

To solve this, we took the same stars (i.e. the ones in the outer disc at 10 Gyr), and computed the fraction which was born in the inner disc defined with respect to the break at their time of birth. This fraction however depends strongly on the value taken for the break radius, since the break is often located near the end of structures such as spirals (Laine et al. 2014; Paper IV), which are high star formation areas (A16 for simulations and e.g. Silva-Villa & Larsen 2012 for observations). Besides, the break radius can be difficult to measure precisely at early times (a few Gyr after the merging). We thus defined errorbars for the estimated break position at each time step for every simulation, and excluded all the particles born closer to the break radius than these errorbars. To make sure our 10 Gyr outer disc definition is also reliable, we defined the particles of the outer disc as the ones located beyond the external errorbar of the break radius.

To exclude the effect of radial displacements due to radial oscillations of stars in their orbit, we chose to use R_G – the guiding radius of each star – instead of their regular radius to derive their position with respect to the break. R_G is the radius of the circular orbit associated to the angular momentum of a given star, and can be derived by solving the equation:

$$R_G = \frac{L_z}{v_{circ}(R_G)}, \quad (5)$$

where L_z is the vertical component of the angular momentum of the star, and v_{circ} is the circular velocity at the guiding radius.

The fractions of outer disc stars that are born in the inner disc derived with this method cover a wide range of values depending on the simulations, from 10 to 80 per cent. Nevertheless, we find globally lower fractions than the ones from section 5.3, as well as the ones from Roškar et al. (2008, ~ 85 per cent), which can be explained by the fact that the break radius tends to increase with time (see paper IV), so that some stars were born inside the 10 Gyr break but outside their birth time break, and thus should be considered as being born in the outer disc. Note that these low fractions can not be explained by our choice to take the guiding radius instead of the regular radius, or to exclude the stars within the errorbars of the break radius: we performed the same analysis using the radius instead of the guiding radius, and also keeping the particles inside the errorbars, and found similar results in both cases.

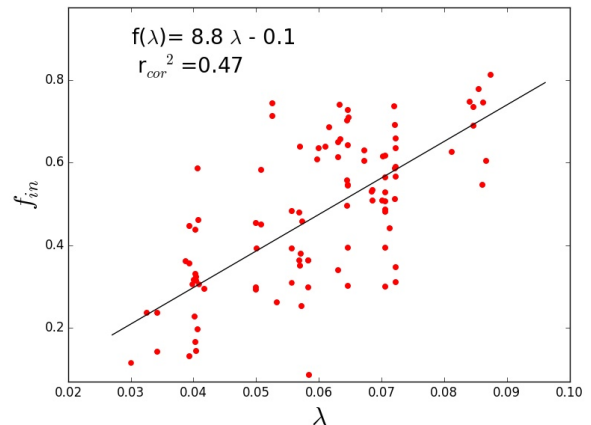


Figure 13. Fraction of outer disc stars which were born in the inner disc, as a function of the spin parameter λ , for sample A+B. For each star, the inner disc is defined here with respect to the break radius derived at its time of birth, as explained in section 5.4.

To understand the spread of values derived for the fraction of stars born in the inner disc, we tried to plot these fractions again versus the spin parameter λ (taken for all the components, 1 Gyr before the merging) in Fig. 13. Although having a large scatter (probably because of the sensitivity of the values to the break location and its errorbars, and the difficulty to define them precisely at early times), this plot shows again an increasing trend of the fractions with λ . Therefore, galaxies with high angular momentum will have an outer disc which is populated by a majority of stars coming from the inner disc, whereas in low angular momentum galaxies, stars in the outer disc will mostly be born in the outer disc. It is important to note that the trend found in Fig. 13 involves the fraction of stars, i.e. relative and not absolute numbers. It thus does not imply that low angular momentum galaxies form more stars in their outer parts, since the number of stars in the outer disc is different in every simulation.

We thus have simulations which have outer discs formed mostly by radial migration, but with a significant amount of stars in the outer parts which were born in the outer disc. We conclude that not taking into account the fact that the break radius changes with time, can lead to overestimating the fraction of stars born in the inner disc in the context of radial migration. Therefore, the picture of outer disc stars mostly coming from the inner disc has to be used with caution, since it depends on the angular momentum of the galaxy. Only galaxies with high spin parameter λ ($\lambda > 0.08$ in our simulations) seem to be able to have about 80 per cent of their outer disc stars born in the inner disc. In galaxies with average or yet lower angular momentum ($\lambda < 0.06$ in our simulations) this fraction drops below 50 per cent, disclaiming the inner disc as the main origin of the outer disc stars.

6 SUMMARY AND CONCLUSION

For this series of papers we ran a sample of high resolution simulations of which three fiducial cases were described in A16, where more general information on the runs was also given. It was shown there that after a merging, a new disc forms in the remnant from gas accreting from the halo. In this paper, we used subsamples derived as described in section 2.1. We derived the stellar radial density profiles of the remnants at the end of all the simulations, and found downbending (type II) profiles. We then derived the corresponding inner and outer disc scalelengths, as well as the break radius. We used the spin parameter λ computed 1 Gyr before the merging to have a definition of the angular momentum consistent for all our simulations. Plotting for our sample the values derived from the radial density profiles fits as a function of λ , we found that the inner, the outer scalelength and the break radius increase with λ . Therefore, both the inner and the outer discs are larger for higher angular momentum systems.

To explain how the initial orbit- and halo-dominated spin parameter λ of the merging system can affect the properties of the final remnant disc (mostly composed of stars born after the merging), we looked at the angular momentum redistribution in our simulations. The scalelengths and break radius correlate with the baryonic angular momentum of the disc, suggesting a link between the latter and the initial angular momentum. To understand how the angular momentum of the disc was acquired, we investigated the transfers of the baryonic matter and angular momentum between the halo and the disc, after making sure that the total baryonic angular momentum is conserved. In the framework of disc galaxy formation from a major merger of two progenitors with extended gas-rich haloes (A16), it is easy to understand that the gaseous halo gives angular momentum to the disc by accreting its gas onto it. We showed this in two fiducial simulations with different λ values, with the halo gas gradually losing a fraction of its mass and angular momentum to the stellar disc, by gas accretion and star formation. We further found that haloes with higher initial total angular momentum (or λ) will create final discs with higher angular momentum, and larger scalelengths and break radius.

Naturally this scenario is only valid for an isolated system with no interactions with the environment. Thus our results, as well as those of other dynamical (and thus necessarily idealised) simulations, can not be straightforwardly extended to a cosmological context, since interactions with environment could interfere with the angular momentum exchanges between the gaseous halo and the baryonic disc.

The correlations of the scalelengths and the break radius with λ are robust and do not change with the time at which we fit the radial density profiles, or the time used to compute λ . Furthermore, simulations of isolated galaxies follow the same trends, so that our results should be valid for discs formed both in isolation and in major mergers. In some simulations, the spin axes of the protogalaxies are tilted, and we showed that the spin axis orientations of the two merging protogalaxies do not seem to play a role in this analysis.

We also included in the correlations a sample of 67 merger simulations with total masses lower or higher than

the simulations from the main sample. Although the evolution time-scale of these simulations is also different, we found that these simulations (which have total masses reasonably close to our main sample) fit well with the others in the correlations, and thus added them to the sample.

We analysed the outer disc origin, and found that the stars ending up in the outer disc were mostly born at smaller radii (~ 95 per cent), suggesting inside-out migration as the main formation driver for the outer disc, in good agreement with previous work on galaxies formed in isolation (Roškar et al. 2008). To see the effect of the angular momentum on this migration, we computed the distance radially travelled by the stars towards the outer disc, and plotted it against the spin parameter λ for the simulations of our sample. We found a clear correlation, galaxies with higher angular momentum having larger inside-out migration distances.

We also showed that to study the origin of the outer disc, it is necessary to take into account the fact that the break location changes with time, so as to avoid overestimations of the fraction of stars born in the inner disc. While ~ 80 per cent of the outer disc stars were born inside the break derived at $t=10$ Gyr, this fraction can take lower values (under 50 per cent) using the time dependent break, which sets doubt on the picture of the outer disc formed mainly from the inner disc. This fraction depends on the angular momentum, and is higher in high angular momentum galaxies. Thus, in some low angular momentum systems, this fraction can drop to values even lower than 20 per cent.

We can thus conclude that the angular momentum is a key parameter in the creation of disc structures, as it affects radial migration, and can explain the large range of values observed for the inner and outer scalelengths in disc galaxies of a given mass.

ACKNOWLEDGEMENTS

We thank Jean-Charles Lambert for computer assistance, and the referee for useful suggestions. This work was supported in part by the Polish National Science Centre under grant 2013/10/A/ST9/00023, and was granted access to the French HPC resources of [TGCC/CINES/IDRIS] under the allocations 2014-[x2014047098], 2015-[x2015047098] and 2016-[x2016047665], made by GENCI, as well as the HPC resources of Aix-Marseille Université financed by the project Equip@Meso (ANR-10-EQPX-29-01) of the program « Investissements d’Avenir » supervised by the Agence Nationale de la Recherche.

REFERENCES

- Athanassoula E., Rodionov S., Peschken N., Lambert J.C., 2016, ApJ, 821, 90 (A16)
- Azzollini R., Trujillo I., Beckman J. E., 2008, ApJ, 684, 1026
- Bakos J., Trujillo I., 2012, preprint (arXiv:1204.3082)
- Comerón S. et al., 2012, ApJ, 759, 98

- Dalcanton J. J., Spergel D.N., Summers F. J., 1997, *ApJ*, 482, 659
- Debattista V. P., Mayer L., Carollo C. M., Moore B., Wadsley J., Quinn T. R., 2006, *ApJ*, 645, 209
- Elmegreen B. G., Hunter D. A., 2006, *ApJ*, 636, 712
- Elmegreen B. G., Struck C., 2013 *ApJ*, 775, L35
- Elmegreen B. G., Struck C., 2016, *ApJ*, 830, 115
- Erwin P., Beckman J. E., Pohlen M., 2005, *ApJ*, 626, L81
- Erwin P., Pohlen M., Beckman J. E., 2008, *AJ*, 135, 20
- Fathi K., Gatchell M., Hatziminaoglou E., Epinat B., 2012, *MNRAS*, 423, L112
- Ferguson A. M. N., Clarke C. J., 2001, *MNRAS*, 325, 781
- Freeman K. C., 1970, *ApJ*, 160, 811
- Gunn J. E., 1982, in *Astrophysical Cosomology Proceedings*, 233
- Gutiérrez L., Erwin P., Aladro R., Beckman J. E., 2011, *ApJ*, 142, 145
- Hammer F., Flores H., Puech M., Yang Y. B., Athanassoula E., Rodrigues M., Delgado R., 2009, 507, 1313
- Herpich J. et al., 2015a, *MNRAS*, 448, 99
- Herpich J., Stinson G. S., Rix H. W., Martig M., Dutton A. A., 2015b, preprint (arXiv:1511.04442)
- Herpich J., Tremaine S., Rix H. W., 2016, preprint (arXiv:1612.03171)
- Kim J., Lee J., 2013, *MNRAS*, 432, 1701
- Kim T. et al. 2014, *ApJ*, 782, 64
- Laine J. et al. 2014, *MNRAS*, 441, 1992
- Lin D. N. C., Pringle J. E., 1987, *ApJL*, 320, L87
- Muñoz-Mateos J.C., Boissier, S., Gil de Paz, A., et al. 2011, *ApJ*, 731, 10
- Muñoz-Mateos J.C. et al., 2013, *ApJ*, 771, 59
- Peebles P.J.E., 1969, *ApJ*, 155, 393
- Perez I., 2004, *A&A*, 427, L17
- Pohlen M., Dettmar R. J., Lütticke R., Aronica G., 2002 *A&A*, 392, 807
- Pohlen M., Trujillo I., 2006, *A&A*, 454, 759
- Radburn-Smith D. J. et al., 2012, 753, 138
- Rodionov S. A., Athanassoula E., Peschken N., 2017, preprint arXiv:1701.02685 (R17)
- Roškar R., Debattista V. P., Stinson G. S., Quinn T. R., Kaufmann T., Wadsley J., 2008, *ApJ*, 675, L65
- Schaye J., 2004, *ApJ*, 609, 667
- Sheth K. et al., 2010, *PASP*, 122, 1397
- Silva-Villa E., Larsen S. S., 2012, *A&A*, 537, A145
- Springel V., 2005, *MNRAS*, 364, 1105
- Springel V., Hernquist L., 2002, *MNRAS*, 333, 649
- Springel V., Hernquist L., 2003, *MNRAS*, 339, 289
- Struck C., Elmegreen B. G. 2017, *MNRAS*, 464, 1482
- van der Kruit P.C., 1979, *A&AS*, 38, 15
- Yoshii Y., Sommer-Larsen J., 1989, *MNRAS*, 236, 779
- Younger J. D., Cox T. J., Seth A. C., Hernquist L., 2007, *ApJ*, 670, 269
- Zheng Z. et al., 2015, *APJ*, 800, 120